Properties of liquid nickel: A critical comparison of EAM and MEAM calculations

F. J. Cherne and M. I. Baskes
Los Alamos National Laboratory, MST-8 Structure and Property Relations, MS G755, Los Alamos, New Mexico 87545

P. A. Deymier
The University of Arizona, Department of Materials Science and Engineering, Tucson, Arizona 85721

(Received 7 June 2001; revised manuscript received 20 August 2001; published 19 December 2001)

In this paper, we compare a variety of properties of liquid nickel calculated with two different embedded atom model functions [J. Cai and Y. Y. Ye, Phys. Rev. B **54**, 8398 (1996); M. I. Baskes, J. I. Angelo, and N. R. Moody, in *Hydrogen Effects on Material Behavior*, edited by N. R. Moody and A. W. Thomson (The Minerals, Metals, and Materials Society, Warrendale, PA, 1995)] and four variations of the modified embedded atom (MEAM) model [M. I. Baskes, Mater. Chem. Phys. **50**, 152 (1997)]. We report calculated values of the melting point and structure factors for each of the representative potentials. We calculate via equilibrium molecular dynamics the shear viscosity and self-diffusion coefficient. This study shows that the short-ranged MEAM potential can give a representative picture of liquid nickel.

DOI: 10.1103/PhysRevB.65.024209 PACS number(s): 61.20.Ja, 61.25.Mv, 64.70.Dv, 66.20.+d

I. INTRODUCTION

There is a great deal of interest in predicting the structure and transport properties of liquid metals.[1–16] The approaches that have been used to study liquid metals include the embedded atom method (EAM),[1–9] the tight-binding method,[10,11] and *ab initio* techniques.[12–16] Each of these methods has been used to study the structure of liquid nickel; however, only the prior two methods have been used to study the transport properties of liquid nickel. One motivation behind studying liquid metals stems from the need for reliable estimates of transport properties. Looking at one transport property, viscosity, the experimental values for liquid nickel at 1750 K range from 4.4 mPa s to 6.2 mPa s.[17] Experimental values for the self-diffusion coefficient of liquid nickel to our knowledge are nonexistent.

Both EAM (Ref. 18) and the modified embedded atom method[19] (MEAM) are a semiempirical representation of transition metals based on density functional theory. The EAM has been applied to the calculation of a variety of properties of perfect and defective (free surfaces, point defects, grain boundaries, dislocations, etc.) bulk metals and alloys as a function of temperature and pressure.[20] A MEAM arose out of the observation that angular forces are necessary to explain the behavior of non-fcc materials.[19] A recent model for tin[21] was able to quantitatively predict the transition between the α and β phases of tin, besides giving reasonable estimates for the melting point.

The applicability of the EAM for the study of liquid metals is well documented in the literature. Foiles[1] showed that liquid transition metals could be modeled with EAM potentials. For the study of nickel, a number of EAM potentials for nickel exist.[22–27] Liquid nickel has been studied with the Voter-Chen potential[6–9] and Johnson's first nearest-neighbor potential.[2] In addition, the viscosity of liquid nickel has been calculated utilizing the Cai-Ye potential.[5] However, because of the recent success of the MEAM in modeling complex materials, we chose to compare the liquids predicted by the MEAM with other EAM potentials.

Although a number of EAM potentials exist, most of the research efforts to date used early EAM potentials (pre-1990) to study the properties of liquid nickel. For this study, we chose to utilize more recent EAM (Refs. 22–24) and MEAM potentials for nickel.[28] These potentials describe the solid properties of nickel better than some of the earlier potentials developed. Thus we intend to provide a critical analysis of these potentials as applied to liquid nickel. The properties to be examined include structure factors, melting points, and transport coefficients (self-diffusivity and viscosity).

II. EAM AND MEAM POTENTIALS

The embedded atom method, as first proposed by Daw and Baskes,[18,29,30] is a semiempirical many-body potential, based on density functional theory. The EAM suggests, in part, that the energy required to place an impurity atom in a lattice is determined by the electron density at that site, irrespective of the source of the electron density. The general form for the total energy is given by[20]

$$E_{total}=\sum_i F(\rho_i)+\frac{1}{2}\sum_i\sum_j \phi(r_{ij}), \tag{1}$$

where ρ_i is the electron density at the ith nucleus resulting from the atomic electron densities of the neighboring atoms, $F(\rho_i)$ is the embedding function, and $\phi(r_{ij})$ is a pair potential term. ρ_i is determined by

$$\rho_i=\sum_{j\neq i} f(r_{ij}), \tag{2}$$

where $f(r_{ij})$ is the electron density due to the jth particle. Both the embedding function and the pair potentials are found empirically, fitting some functional form to the solid properties of the lattice constant, cohesive energy, elastic constants, vacancy formation energy, etc. The EAM assumes that the electron density is spherically symmetric, whereas the MEAM assumes that the background electron density is a function of some angular-dependent ''partial electron densi-

ties.'' Baskes[19,28] gives a more detailed description of the angular-dependent electron densities.

We utilized two different EAM potentials in this study: the EAM of Angelo *et al.*[23,24] (A-EAM) and the Cai-Ye[22] (CY-EAM) potentials. The functional forms of each of these potentials are physically different. The methodology in the fitting the solid database parameters also differs. We summarize in the following subsections the functional forms for the electron density, the embedding function, and pair function for both the EAM potentials and MEAM potentials.

A. Potential of Angelo *et al.*

Angelo *et al.*[23,24] chose the pair potential to be given by the following expression

$$\phi(r_{ij})=c_1[e^{-2c_2(r_{ij}-c_3)}-2e^{-c_2(r_{ij}-c_3)}]f_{cut}(r_{ij})+c_{10}f(r_{ij}), \tag{3}$$

where c_1, c_2, c_3, and c_{10} are fitted parameters, $f(r_{ij})$ is the electron density due to the jth atom, and f_{cut} is given by

$$f_{cut}(r_{ij})=\exp\left(\frac{1}{r_{ij}-r_{cut}}\right), \tag{4}$$

This f_{cut} forces the pair potential as well as the electron density (to be shown later) to zero beyond a certain distance r_{cut}. The value of r_{cut} is 4.84 Å, which is an adjustable parameter that provides the best match between the calculated and experimental data.

The total electron density ρ_i given by Eq. (2) requires the summation of $f(r_{ij})$ which was taken to follow the functional form of Chen *et al.*[31] and is given by

$$f(r_{ij})=c_4 r_{ij}^6(e^{-c_5 r_{ij}}+2^9 e^{-2c_5 r_{ij}})f_{cut}(r_{ij}), \tag{5}$$

where r_{ij} is the distance between the ith and jth atoms, c_4 and c_5 are fitted constants, and f_{cut} is given by Eq. (4).

Having chosen the functional forms for the electron density and the pair potential, the embedding energy function is determined as

$$F(\rho_i)=E(a)-\frac{1}{2}\sum_{i,j}\phi_{ij}(r_{ij}), \tag{6}$$

where $\phi_{ij}(r_{ij})$ is given by Eq. (3) and $E(a)$ is the energy given by the equation of state of Rose *et al.*,[32] which is

$$E(a)=-E_{sub}(1+a^*)e^{-a^*}, \tag{7}$$

where E_{sub} is the sublimation energy. The quantity a^* is a measure of the deviation from the equilibrium lattice constant a_0 and is given by

$$a^*=\frac{\left(\frac{a}{a_0}-1\right)}{\left(\frac{E_{sub}}{9B\Omega}\right)^{1/2}}. \tag{8}$$

Here, Ω is the equilibrium atomic volume, B is the bulk modulus, and a is the current lattice constant. The parameters used in this study were described in Ref. 24.

B. Cai-Ye potential

Cai and Ye[22] approached the embedded atom method by assuming that the embedding function should match the universal binding energy expression described by Banarjea and Smith[33] and that the pair potential should match in functional form the equation of state of Rose *et al.*[32] Angelo *et al.*, on the other hand, required the total energy to obey the equation of state of Rose *et al.* The embedding function for the CY-EAM is defined by the equation

$$F(\rho)=-F_0\left[1-n\ln\left(\frac{\rho}{\rho_e}\right)\right]\left(\frac{\rho}{\rho_e}\right)^n+F_1\left(\frac{\rho}{\rho_e}\right), \tag{9}$$

where ρ_e is the equilibrium electronic density (for a perfect fcc crystal it is approximately 12), F_0 is defined as the cohesive energy minus the energy of vacancy formation, F_1 is an adjustable parameter, ρ is the electron density given by Eq. (2), and n was taken as 0.5. They chose $f(r_{ij})$ to be a simple exponentially decreasing function of r_{ij} given by

$$f(r)=f_e\ \exp[-\chi(r_{ij}-r_e)], \tag{10}$$

where r_e is the equilibrium nearest-neighbor distance, f_e is a scaling constant taken as one for pure substances, and χ is a fitted parameter.

As mentioned above the pair potential was taken to be of the form of the equation of state of Rose *et al.*, more specifically

$$\phi(r_{ij})=-\alpha\left[1+\beta\left(\frac{r}{r_a}-1\right)\right]\exp\left[-\beta\left(\frac{r}{r_a}-1\right)\right], \tag{11}$$

where α, β, and r_a were taken as adjustable parameters. The cutoff distance chosen for the parametrization was set to be 1.65 times the lattice parameter a_0. This represents a distance (5.8 Å) between the fifth and sixth nearest-neighbor distances. The resulting fitted parameters for nickel given by Cai and Ye[22] were utilized in this work.

C. Modified embedded atom method potential

The modified embedded atom method is an extension of the EAM which follows Eq. (1) yet includes an angular-dependent electron density function. Historically MEAM potentials have been chosen to be short range whereas EAM potentials usually are longer range. For a complete description of the MEAM formalism we refer the reader to the papers by Baskes.[19,28]

The background electron density in the MEAM is taken as

$$\overline{\rho}=\rho_i G(\Gamma), \tag{12}$$

where ρ_i is the EAM electron density given in Eq. (2) and $G(\Gamma)$ captures the angular dependence. The scalar Γ is given by a weighted sum of the squares of partial electron densities scaled by ρ_i. Each partial electron density captures a differ-

ent aspect of the local atomic environment; e.g., the *s* component represents volume, the *p* component represents mirror symmetry, the *d* component represents shear, and the *f* component represents inversion symmetry. The various forms chosen for the function *G* are discussed in Baskes[28] and will be discussed further below. Each partial electron density is proportional to an atomic electron density. The atomic electron densities are given by simple exponentials with decay constant $\beta^{(l)}$, $l=0-3$.

A many-body screening function was given by Baskes[28] which we summarize here. The screening function between atoms *i* and *k* depends on all of the other atoms *j* in the system through an equation such as

$$S_{ik}=\prod_{j\neq i,k} S_{ijk}, \tag{13}$$

where S_{ijk} is calculated using a simple elliptical construction. Consider the ellipse passing through atoms *i*, *j*, and *k* where the *x* axis of the ellipse is determined by *i* and *k*. The equation for the ellipse is given by

$$x^2+\frac{1}{C}y^2=\left(\frac{1}{2}r_{ik}\right)^2, \tag{14}$$

where the parameter *C* is determined by

$$C=\frac{2(X_{ij}+X_{jk})-(X_{ij}-X_{jk})^2-1}{1-(X_{ij}-X_{jk})^2}, \tag{15}$$

where $X_{ij}=(r_{ij}/r_{ik})^2$ and $X_{jk}=(r_{jk}/r_{ik})^2$. The *r*'s are the distance between the respective atoms. We defined the screening factor to be a smooth function of *C*:

$$S_{ijk}=f_c\left[\frac{C-C_{min}}{C_{max}-C_{min}}\right], \tag{16}$$

where C_{min} and C_{max} are material-dependent parameters and the smooth cutoff function is

$$f_c(x)=\begin{cases} 1, & x\geqslant 1, \\ [1-(1-x)^4]^2, & 0<x<1, \\ 0, & x\leqslant 0. \end{cases} \tag{17}$$

For this paper, we utilized each of the nickel potentials developed by Baskes.[28] We chose to increase the value for the cutoff radius r_c from 4 to 4.5 Å in order to maintain constant energy within the liquid. The four potentials will be referred to as Ni1, Ni2, Ni3, and Ni4 to correspond with the four MEAM potentials given by Baskes.[28] Tabulated in Table I are the unique parameters, $\beta^{(1)}$, $\beta^{(3)}$, C_{min}, and the function for $G(\Gamma)$ for each of these model potentials.

TABLE I. Parameters for MEAM potentials.

Potential	$\beta^{(1)}$	$\beta^{(3)}$	C_{min}	$G(\Gamma)$
Ni1	2.2	2.2	2.0	$\sqrt{1+\Gamma}$
Ni2	2.2	2.2	2.0	$\frac{2}{1+\exp(-\Gamma)}$
Ni3	1.5	1.5	2.0	$\frac{2}{1+\exp(-\Gamma)}$
Ni4	1.5	1.5	0.8	$\frac{2}{1+\exp(-\Gamma)}$

III. COMPUTATIONAL DETAILS

A. Transport properties

In order to calculate the various transport properties given in this paper, we used the Green-Kubo[34,35] method as developed by McQuarrie.[36] The transport properties are derived from the continuum equations of fluid dynamics, such as the Navier-Stokes equation for viscosity or Fick's laws of diffusion. The derivation provides a direct relation between the microscopic autocorrelation function (ACF) measured in an equilibrium system to the macroscopic transport quantity.

The autocorrelation function that one obtains for the diffusion coefficient is given by the following expression[36]

$$D=\frac{1}{3N}\int_0^\infty \left\langle \sum_{j=1}^{N} \vec{v}_j(0)\cdot\vec{v}_j(\tau)\right\rangle d\tau, \tag{18}$$

where *N* is the number of atoms, $\vec{v}_j(0)$ is initial velocity vector for the *j*th particle, and $\vec{v}_j(\tau)$ is the velocity vector at some later time τ. The average is taken over different time origins.

A similar expression for the shear viscosity exists relating the shear viscosity to the off-diagonal terms of the stress tensor. The resulting expression is

$$\eta=\frac{1}{Vk_bT}\int_0^\infty \langle J(0)J(\tau)\rangle d\tau, \tag{19}$$

where *V* is the volume, k_b is Boltzmann's constant, *T* is the absolute temperature, and *J* is defined by

$$J_{\alpha\beta}=\sum_{j=1}^{N}\left(\frac{p_{\alpha j}p_{\beta j}}{m_j}+\beta_j F_{j\alpha}\right) \tag{20}$$

and is related to one component of the off-diagonal term of the stress tensor, $\sigma_{\alpha\beta}$, where $\alpha\beta$ equals xz, xy, yz, yx, zx, or zy. $p_{\alpha j}$ and $p_{\beta j}$ are the momenta of particle *j* in the α and β directions, respectively, β_j is the β component of the *j*th particle position vector, and $F_{j\alpha}$ is the α component of the force. Again we take the average of the off-diagonal terms at different time origins.

In order to obtain reliable average values for Eqs. (18) and (19) we utilize a method of overlapping-time-interval correlation averages.[37] This method allows one to store in memory a series of individual correlation functions $A(0)A(\tau)$ (where *A* is the quantity of interest—for example, the velocity or off-diagonal terms of the stress tensor), spaced apart by some time. The time spacing is determined such that there is no correlation between the initial correlation function and the second correlation function. This significantly shortens the computational time while getting meaningful statistical averages.

The results for the self-diffusivity and the shear viscosity are calculated using an average of 4000 individual correlation functions spaced 0.1 ps apart with a total time for the correlation function being 1 ps. Longer correlation functions as well as including more correlation functions in the average did not significantly alter the resulting values. For each autocorrelation function calculated, the simulations lasted approximately 400 ps. A total of three to five autocorrelation functions were subsequently averaged to obtain the values presented. The errors for the calculated diffusivity data were less than 2%. The estimated errors in the shear viscosity data were less than 7%. These simulations were run using a microcanonical ensemble (constant N, V, and E). The volume was selected in such a way that the average pressure equaled zero. Each of these simulations contained 1372 atoms. We evaluated the effect of system size on our calculations and found that 1372 atoms was the optimal size for statistically meaningful results and computational feasibility.

B. Other properties

We calculated the structural parameters through a series of isobaric-isothermal simulations at 1775 K and zero pressure for each of the nickel potentials. Temperature was controlled using a standard Nosé-Hoover thermostat[38,39] with a time constant of 0.1 ps. A radial distribution function was calculated for 150 different configurations of 10 976 atoms. A Fourier transform of the radial distribution function was evaluated to obtain the structure factors we present in Sec. IV.

The melting point was calculated using the moving interface method.[40] This method is a two-phase simulation method that measures the velocity of the interface for a variety of temperatures. The simulations were allowed to expand and contract at zero constant pressure while temperature was held fixed away from the moving interface. This technique provides reasonable estimates of the melting point. A series of simulations bracketing the assumed melting temperature was run while determining the velocity of the interface. The total length of the simulations was 25 ps with output times being 0.1 ps. The velocities were plotted with respect to the temperature of the uncontrolled temperature region. The melting point was taken as the temperature at which the velocity equaled zero.

IV. RESULTS AND DISCUSSION

Following the two-phase simulation method described above, the melting points for each of the potentials were obtained. Tabulated in Table II are the melting points. The experimental melting point of nickel is 1726 K. It is noticed that Ni1, Ni2, and Ni3 all have similar melting points. Comparing the resulting melting points of liquid nickel predicted through MEAM calculations, the value of C_{min} appears to have a strong effect on the melting temperature (see Table I). It was noticed by Baskes[28] that the selection of the C_{min} also affects the linear expansion coefficient for the solid. The selection of the form for the background electron density $G(\Gamma)$ appears to have a minimal effect in changing the melting temperature within the errors associated with the method of determining the melting temperature.

TABLE II. Calculated melting points and atomic densities for the EAM and MEAM potentials. Experimental density (Ref. 41) at $T=1773$ K is 0.0792 atoms/Å^3 and the experimental melting point is $T=1726$ K.

Potential	T_m (K) ± 25 K	ρ at $T=1775$ K (atoms/Å^3)
A-EAM	1478	0.0781
CY-EAM	1536	0.0785
Ni1	1880	0.0778
Ni2	1825	0.0780
Ni3	1890	0.0783
Ni4	1570	0.0781

Also included in Table II are the zero-pressure densities at 1775 K. These densities are slightly lower than the experimental density.[41] The CY-EAM potential appears to be the closest to the experimental density. The furthest from experimental density was that of Ni1 which is 1.8% less than that of the experimental. Thus each of the potentials predict a zero-pressure density very close to the experimental results.

In Fig. 1, the structure factor for each of the potentials evaluated within this paper is plotted. The experimental results indicated by the open circles were obtained from Waseda and Ohtani.[41] The lines in the figure represent the structure factor from the potentials. Each of the potentials appears to fit the experimental data well. Even though each of the potentials predicts the structure well, the structures for MEAM Ni1 and MEAM Ni2 appear to have longer-range correlations. In other words, the second and third peaks are

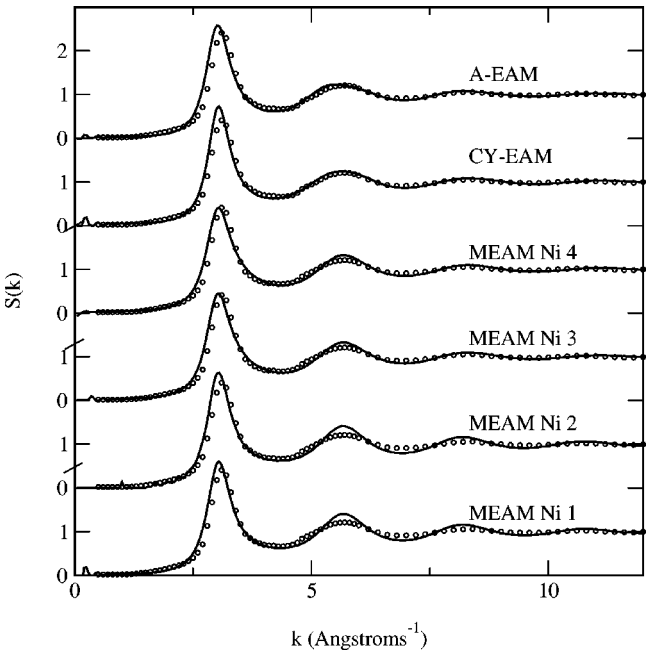

FIG. 1. Structure factor of liquid nickel. Lines represent the calculated structure factor for EAM and MEAM liquid nickel; symbols represent the experimental structure factor data (Ref. 41).

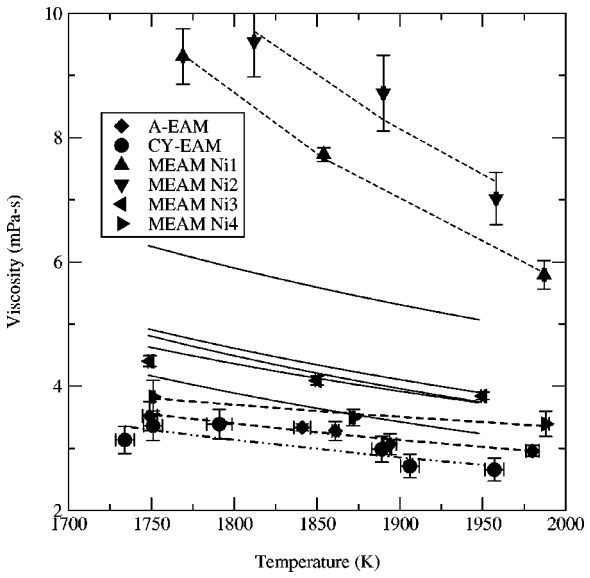

FIG. 2. Viscosity of liquid nickel as a function of temperature. Solid lines represent experimental data from the early 1950s to the late 1960s (Ref. 17). Dashed lines correspond to an Arrhenius best-fit curve through calculated data points.

more pronounced. The position of the first peaks of the A-EAM and CY-EAM appears to be shifted slightly from the experimental data points. Comparing each of the structure factor curves in Fig. 1, it is noticed that the structure factors are nearly identical for MEAM Ni1 and MEAM Ni2, MEAM Ni3 and MEAM Ni4, and A-EAM and CY-EAM. Thus, referring to the table for the MEAM potentials, Table I, one sees that the structure factor appears to be controlled by the selection of the $\beta^{(1)}$ and $\beta^{(3)}$ parameters.

In Fig. 2 we report the viscosity results compared to the experimental viscosities from the 1950s and 1960s found in Iida and Guthrie.[17] The solid lines represent the experimental results; our results are illustrated with symbols and the dashed lines. The dashed lines represent an Arrhenius-like function through the data. The temperature uncertainty arises from the temperature fluctuations within the simulations. In a prior paper,[5] we reported larger fluctuations in the values for the viscosity. Here we reduced the deviations by averaging more individual correlation functions. Furthermore, we ensured that the spacing between the correlation functions was such that each correlation function was significantly decayed before overlapping the next correlation function. The overall values of the viscosity were not significantly affected, however. The errors associated with the calculations were reduced to less than $\pm 7\%$.

There have been other calculations for the viscosity of liquid nickel based on the Voter-Chen EAM potential.[6–8] Besides the difference in the potential the methodology in their papers differs slightly in that they calculated the Green-Kubo viscosities at the experimental density rather than the zero-pressure densities used here. This fundamental difference could dramatically affect the viscosity obtained. For instance, one of the authors[42] ran several calculations for liquid nickel examining the effect of the density upon the shear viscosity and observed that decreasing the density by 2% decreased the shear viscosity by nearly 10%. Thus it is inconsistent to calculate the shear viscosity using experimental densities rather than the zero-pressure densities predicted by the model.

TABLE III. Viscosity parameters assuming Arrhenius behavior for each potential. The units of η_0 are mPa s and of E_a are eV.

	Viscosity		
Potential	η_0	E_a	E_a/kT_m
A-EAM	3.61	0.224	1.76 ± 0.03
CY-EAM	3.38	0.277	2.09 ± 0.03
Ni1	10.36	0.656	4.05 ± 0.05
Ni2	11.76	0.601	3.82 ± 0.05
Ni3	4.48	0.200	1.23 ± 0.05
Ni4	3.84	0.157	1.16 ± 0.03
Expt. range	4.2–6.4	0.311–0.374	2.09–2.51

Over the limited temperature range we studied, the viscosity appeared to follow an Arrhenius relationship

$$\eta = \eta_0 \exp\left[\frac{E_a}{k_b}\left(\frac{1}{T}-\frac{1}{T_m}\right)\right], \tag{21}$$

where η_0 is the viscosity at the experimental melting point, k_b is Boltzmann's constant, and E_a is the activation energy. In Table III, we present the values for the activation energies of each process as well as the prefactors for each of the potentials studied here. It is difficult to compare these values to experimental data, in part, due to the difficulty in experimentally measuring viscosity at high temperatures. The calculated activation energy for the viscosity of MEAM Ni3, Ni4, A-EAM, and CY-EAM is lower than the activation energy from most experimental data by up to a factor of 1.5. The activation energy is higher by a factor greater than 2 for the Ni1 and Ni2 potentials.

The calculated viscosity for MEAM Ni1 and Ni2 appears to overestimate the experimental numbers while the remaining MEAM potentials and the EAM potentials tend to slightly undershoot the experimental numbers. These results could be explained purely from structural arguments. In the literature there exists a relationship that relates the microscopic details of the system to the viscosity through a semi-empirical function of $g(r)$ and the Lindemann frequency ω_L,[17,43]

$$\eta = \frac{8\pi}{9}\omega_L m n_0^2 \int_0^a r^4 g(r)\,dr, \tag{22}$$

where m is the atomic mass, n_0 is the atomic density, and a denotes the first minimum of the radial distribution function. The Lindemann frequency is proportional to the square root of the melting temperature. The Lindemann frequency that we use is 3.75×10^{12} s^{-1} which corresponds to 15.5 meV.[43] We then adjust this value to the melting point of the potential. In Table IV, we compare our viscosity values extrapolated to the potentials melting point to the viscosity calculated from Eq. (22). Comparing the trends with the calculated integral and its resulting viscosity, Eq. (22) ap-

TABLE IV. Viscosity values calculated from Eq. 22. The Lindemann frequency used is equal to $3.75\times10^{12}\sqrt{T_{mcalc}/T_{mexpt.}}$ The units of η, a, and $\int_0^a r^4 g(r)dr$ are mPa s, Å, and Å^5, respectively.

Potential	η_{calc} (T_{mcalc})	$\eta_{semiemp}$ (T_m)	a	$\int_0^a r^4 g(r)dr$
A-EAM	4.65	5.70	3.43	99.0
CY-EAM	4.26	5.82	3.43	98.2
Ni1	7.22	4.27	3.03	66.3
Ni2	9.45	4.23	3.03	66.3
Ni3	3.99	4.97	3.18	75.9
Ni4	4.24	4.29	3.13	72.3

pears to not be a valid expression for our systems. Recall, however, that MEAM Ni1 and MEAM Ni2 had essentially the same structure and compared to the experimental structure factors had greater intensity for the second and third peaks. Perhaps Eq. (22) should be modified to extend to beyond the second and third nearest-neighbor distances. Furthermore, the more intense correlations at longer distances appear to contribute significantly to values for the viscosity.

In Fig. 3, we report the results for the self-diffusion coefficient of liquid nickel as a function of temperature. The solid line in the figure represents the self-diffusivity predicted by Protopapas *et al.*[44] The solid data points are the self-diffusivity calculated in this work. The open symbols represent the self-diffusion calculated by Alemany *et al.*[10] and by Mei and Davenport.[2] Alemany *et al.* utilized a tight-binding potential for their study and Mei and Davenport utilized Johnson's[26] first nearest-neighbor analytical EAM potential. Considering the differences in the potentials, we see consid-

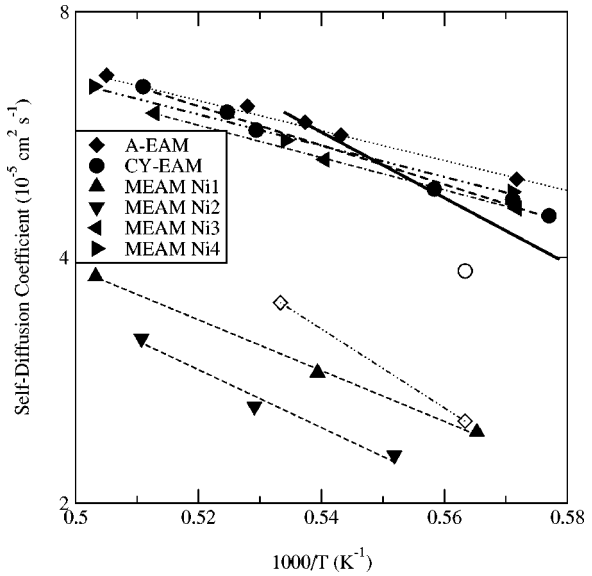

FIG. 3. Self-diffusion coefficient of liquid nickel as a function of temperature. The solid line is the data predicted by Protopapas *et al.* (Ref. 44). Dashed lines correspond to an Arrhenius best-fit curve through calculated data points. The open circle corresponds to data obtained by Mei and Davenport (Ref. 2). Open diamonds are the results of Alemany *et al.* (Ref. 10).

TABLE V. Arrhenius diffusion parameters for each potential. The units of E_a are eV and of D_0 are 10^{-5} cm^2 s^{-1}.

	Self-diffusivity		
Potential	D_0	E_a	E_a/kT_m
A-EAM	56.0	0.364	2.86 ± 0.05
CY-EAM	108.0	0.476	3.59 ± 0.06
Ni1	139.5	0.618	3.80 ± 0.05
Ni2	203.7	0.704	4.47 ± 0.06
Ni3	62.4	0.394	2.42 ± 0.03
Ni4	59.6	0.381	2.81 ± 0.05

erable agreement between the CY-EAM, A-EAM, MEAM Ni3, and MEAM Ni4 potentials. We also see agreement between the MEAM Ni1 and MEAM Ni2 potentials. The self-diffusivity appeared to obey the following Arrhenius-type equation:

$$D=D_0\exp\left(-\frac{E_a}{k_bT}\right), \tag{23}$$

where D_0 is the self-diffusion prefactor. The values for D_0 and E_a appear in Table V. The data predicted by Protopapas *et al.*[44] is comparable in value with the A-EAM, CY-EAM, MEAM Ni3, and MEAM Ni4, yet the slope for the data Protopapas *et al.* is greater. The activation energy for the data of Protopapas *et al.* is 0.818 eV/atom which differs from our activation energies by as much as a factor of 2.

Oftentimes the self-diffusion coefficient is predicted from viscosity data using Stokes-Einstein or Sutherland-Einstein expressions. The Stokes-Einstein relationship is given by

$$D=\frac{k_bT}{6\pi R\eta} \tag{24}$$

and the Sutherland-Einstein expression is

$$D=\frac{k_bT}{4\pi R\eta}, \tag{25}$$

where the atomic radius R is calculated from the atomic volume. Applying both relationships to the Angelo potential, we obtain the results shown in Fig. 4. From the figure, it is observed that the Sutherland-Einstein relationship, Eq. (25), provides a closer agreement to the calculated self-diffusion coefficient. Although the Sutherland-Einstein relationship provides good qualitative predictions for the self-diffusion coefficient for pure liquid metals, one must exercise caution in applying either of the expressions where accurate self-diffusivities are needed.

Examining the functional form of Eqs. (24) and (25), we recognize that the expressions could be generalized as

$$\frac{DR\eta}{k_bT}=\text{const}, \tag{26}$$

where const$=1/6\pi$ and $1/4\pi$ for the Stokes-Einstein and Sutherland-Einstein equations, respectively. In Fig. 5, we plot Eq. (26) for each of the potentials. The lower solid line

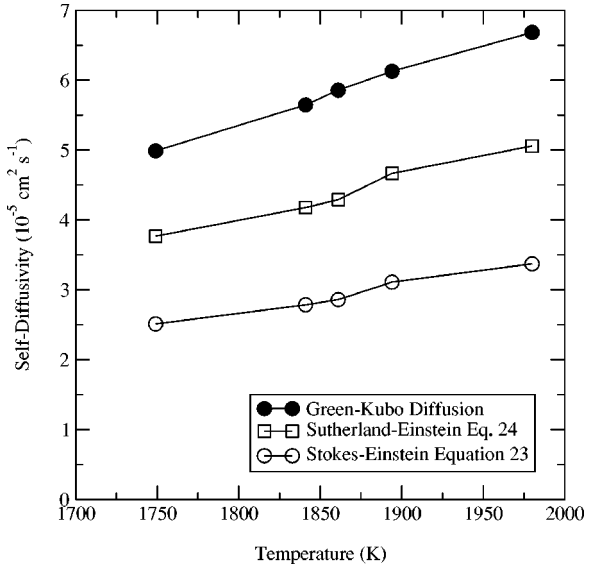

FIG. 4. Self-diffusivity calculated for the potential of Angelo *et al.* A comparison between the Green-Kubo diffusivity, Stokes-Einstein relationship [Eq. (24)], and Sutherland-Einstein relationship [Eq. (25)]. Solid data points are calculated from Green-Kubo relationships. Open squares from Eq. (25). Open circles from Eq. (24).

in the plot represents the constant for the Sutherland-Einstein model, $1/4\pi$. Aside from the data scatter, Eq. (26) does hold for all the potentials except for MEAM Ni1 and MEAM Ni2. Each potential gives a slightly different constant which implies that the constant in Eq. (26) is potential dependent.

Under the assumption that Eqs. (26) and (23) are valid, we plot in Fig. 6 the natural logarithim of η/T as a function of T_m/T. We chose in Fig. 6 to plot with finer detail the experimental data A-EAM, CY-EAM, MEAM Ni3, and MEAM Ni4 for a closer comparison. MEAM Ni1 and

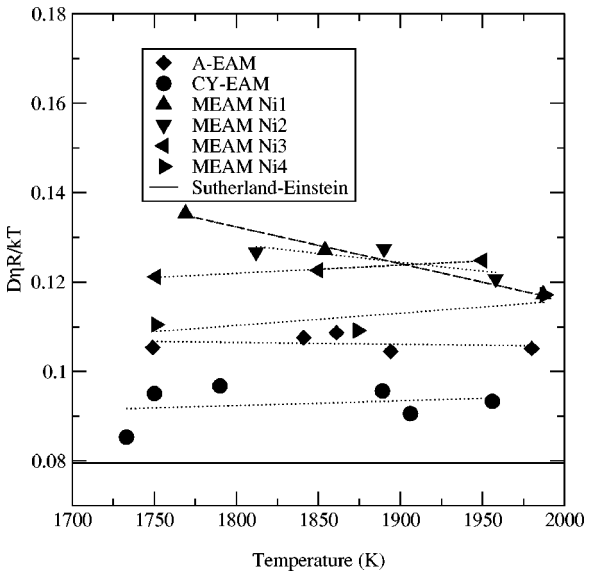

FIG. 5. Plot of Eq. (26) vs temperature. The solid line represents a value constant from the Sutherland-Einstein expression, Eq. (25). Dashed lines are least-squares fits for each data set.

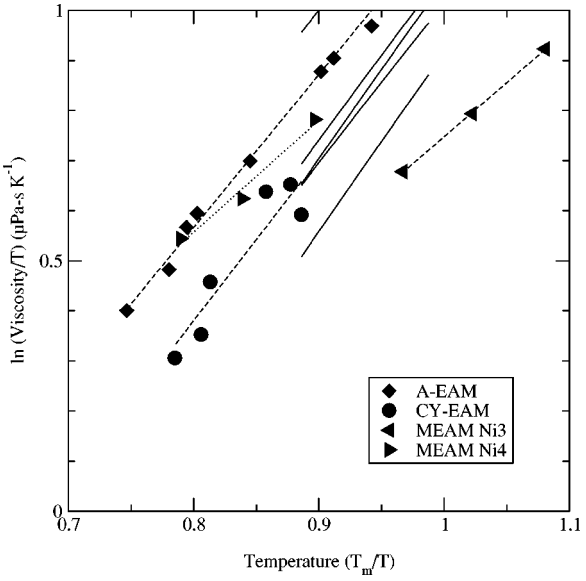

FIG. 6. Plot of the natural logarithim of η/T vs T_m/T. Solid lines represent experimental lines from the 1950s and 1960s. Dashed lines are best fits through the data obtained in this work.

MEAM Ni2 are beyond the range of the graph. T_m is taken as the value found in Table II. For the experimental curves T_m was taken to be 1726 K. With the A-EAM potential we also aquired data below the experimental melting point of 1726 K to see if the trend continued below 1478 K, the prior referenced melting point of the potential. By analyzing our data in this manner, we recognize that each of the EAM and experimental curves have essentially the same slope while the slope of the MEAM Ni3 and Ni4 potentials is slightly lower. This high correlation between the potentials and the experimental points indicates that A-EAM, CY-EAM, MEAM Ni3, and MEAM Ni4 represent nickel very well. Furthermore, considering the errors associated with the method in determining the melting points, A-EAM, CY-EAM, and MEAM Ni4 could very well lie on the same line.

Another approach that has been recently suggested by Dzugotov[45] which relates the self-diffusion coefficient to the excess entropy of the liquid, which is related to the radial distribution function $g(r)$. The relation for the dimensionless diffusion coefficient Dzugotov proposed was

$$D^* = 0.049 e^{S_2}, \tag{27}$$

where S_2 is the excess entropy of the system and is defined as

$$S_2 = -2\pi\rho \int_0^\infty \{g(r)\ln[g(r)] - [g(r)-1]\} r^2 dr, \tag{28}$$

where ρ is the atomic density, r is the radial position, and $g(r)$ is the radial distribution function. Once the dimensionless diffusion coefficient is calculated the actual diffusion coefficient can be calculated using the following relationship:

$$D = D^* \Gamma_E \sigma^2, \tag{29}$$

where σ is the position of the first maximum in the radial distribution function. Γ_E corresponds with the Enskog collision frequency, given by

$$\Gamma_E = 4\sigma^2 g(\sigma)\rho\sqrt{\frac{\pi k_b T}{m}}, \tag{30}$$

where $g(\sigma)$ is the value of the radial distribution function at σ and m is the mass of the atom. D^* exhibits some temperature and potential dependence through the characteristics of $g(r)$ with temperature and potential chosen. To test Dzugotov's universal scaling law, we took the radial distribution function of the Cai-Ye potential at 1725 K and calculated the diffusion coefficient from Dzugutov's expressions for the self-diffusivity. We obtained a diffusion coefficient of 3.52×10^{-5} cm^2/s. The equilibrium molecular dynamics results in a self-diffusivity of 4.50×10^{-5} cm^2/s. Although the self-diffusivities are comparable, these numbers suggest that the universal scaling law might not be universal. In fact, Hoyt *et al.*[46] suggested that the universal scaling law is valid for many-body potentials when the actual excess entropy is used rather than the simple two-body approximation for the excess entropy. Thus we concur with Hoyt *et al.* that the simple two-body approximation to the excess entropy does not provide valid estimates for the self-diffusivity through the universal scaling law.

V. CONCLUSIONS

We have examined a variety of liquid nickel properties predicted from two EAM potentials as well as four MEAM potentials. Of these potentials each gives reasonable structures compared to experimental data. The melting points determined by the moving interface method were in fair agreement for all of the potentials with the potential of Angelo *et al.* yielding the worst results. On the other hand, the other calculated properties of the EAM potential of Angelo *et al.* agree well with the available experimental values. The melting points may be affected by the choice of the C_{min} parameter in the screening function of the MEAM. The self-diffusion coefficient and the viscosity appear to be dependent upon the details of the liquid structure out to the second and third nearest-neighbor distances. In other words, the long-distance correlations appear to increase the viscosity and decrease the diffusion coefficient. In addition, this study extends the work of Foiles[1] by illustrating that MEAM potentials, even though short ranged, describe the structure of the liquids effectively. Of the MEAM potentials for nickel examined, MEAM Ni3 and MEAM Ni4 appear to provide the best agreement with the available experimental data.

[1] S.M. Foiles, Phys. Rev. B **32**, 3409 (1985).
[2] J. Mei and J.W. Davenport, Phys. Rev. B **42**, 9682 (1990).
[3] G.M. Bhuiyan, M. Silbert, and M.J. Stott, Phys. Rev. B **53**, 636 (1996).
[4] G. Bhuiyan and M.A. Khaleque, J. Non-Cryst. Solids **226**, 175 (1998).
[5] F.J. Cherne and P.A. Deymier, Scr. Mater. **39**, 1613 (1998).
[6] M.M.G. Alemany, C. Rey, and L.J. Gallego, Phys. Rev. B **58**, 685 (1998).
[7] M.M.G. Alemany, C. Rey, and L.J. Gallego, J. Chem. Phys. **109**, 5175 (1998).
[8] M.M.G. Alemany, C. Rey, and L.J. Gallego, J. Chem. Phys. **109**, 3568 (1998).
[9] M.M.G. Alemany, C. Rey, and L.J. Gallego, J. Chem. Phys. **111**, 9111 (1999).
[10] M.M.G. Alemany, O. Diéguez, C. Rey, and L.J. Gallego, Phys. Rev. B **60**, 9208 (1999).
[11] L.D. Phuong, A. Pasturel, and D.N. Manh, J. Phys.: Condens. Matter **5**, 1901 (1993).
[12] D. Alfè and M.J. Gillan, Phys. Rev. Lett. **81**, 5161 (1998).
[13] R. Stadler, D. Alfè, G. Kresse, G. de Wijs, and M.J. Gillan, J. Non-Cryst. Solids **250-252**, 82 (1999).
[14] J.L. Bretonnet and N. Jakse, Phys. Rev. B **50**, 2880 (1994).
[15] N. Jakse and J.L. Bretonnet, J. Phys.: Condens. Matter **7**, 3803 (1995).
[16] N. Jakse, J.F. Wax, J.L. Bretonnet, and A. Pasturel, J. Non-Cryst. Solids **207-207**, 434 (1996).
[17] T. Iida and R. I. L. Guthrie, *The Physical Properties of Liquid Metals* (Clarendon Press, Oxford, 1988).
[18] M.S. Daw and M.I. Baskes, Phys. Rev. B **29**, 6443 (1984).
[19] M.I. Baskes, Phys. Rev. B **46**, 2727 (1992).
[20] M.S. Daw, S.M. Foiles, and M.I. Baskes, Mater. Sci. Rep. **9**, 251 (1993).
[21] R. Ravelo and M. Baskes, Phys. Rev. Lett. **79**, 2482 (1997).
[22] J. Cai and Y.Y. Ye, Phys. Rev. B **54**, 8398 (1997).
[23] J.E. Angelo, N.R. Moody, and M.I. Baskes, Modell. Simul. Mater. Sci. Eng. **3**, 289 (1995).
[24] M.I. Baskes, X. Sha, J.E. Angelo, and N.R. Moody, Modell. Simul. Mater. Sci. Eng. **5**, 651 (1997).
[25] A. Voter and S. Chen, in *Characterization of Defects in Materials* edited by R. Siegel, J. Weertman, and R. Sundan, Mater. Res. Soc. Symp. Proc. No. 82 (Materials Research Society, Pittsburgh, PA, 1987), pp. 175–180.
[26] R.A. Johnson, Phys. Rev. B **37**, 3924 (1988).
[27] S.M. Foiles, M.I. Baskes, and M.S. Daw, Phys. Rev. B **33**, 7983 (1986).
[28] M.I. Baskes, Mater. Chem. Phys. **50**, 152 (1997).
[29] M.S. Daw and M.I. Baskes, Phys. Rev. Lett. **50**, 1285 (1983).
[30] M.S. Daw, Phys. Rev. B **39**, 7441 (1989).
[31] S.P. Chen, D.J. Srolovitz, and A.F. Voter, J. Mater. Res. **4**, 62 (1989).
[32] J.H. Rose, J.R. Smith, F. Guinea, and J. Ferrante, Phys. Rev. B **29**, 2963 (1984).
[33] A. Banerjea and J.R. Smith, Phys. Rev. B **37**, 6632 (1988).
[34] M.S. Green, J. Chem. Phys. **20**, 1281 (1952).
[35] M.S. Green, J. Chem. Phys. **22**, 398 (1954).
[36] D. A. McQuarrie, *Statistical Mechanics* (University Science Books, Sausalito, CA, 2000).
[37] D. C. Rapaport, *The Art of Molecular Dynamics Simulation* (Cambridge University Press, Cambridge, UK, 1995).

[38] W.G. Hoover, Phys. Rev. A **31**, 1695 (1985).
[39] S. Nosé, Prog. Theor. Phys. Suppl. **103**, 1 (1991).
[40] M.I. Baskes, Phys. Rev. Lett. **83**, 2592 (1999).
[41] Y. Waseda and M. Ohtani, Phys. Status Solidi B **62**, 535 (1974).
[42] F. J. Cherne III, Ph.D. thesis, The University of Arizona, 2000.
[43] F.J. Bermejo, M.L. Saboungi, D.L. Price, M. Alvarez, B. Roessli, C. Cabrillo, and A. Ivanov, Phys. Rev. Lett. **85**, 106 (2000).
[44] P. Protopapas, H.C. Andersen, and N.A.D. Parlee, J. Chem. Phys. **59**, 15 (1973).
[45] M. Dzugutov, Nature (London) **64**, 1278 (1990).
[46] J.J. Hoyt, M. Asta, and B. Sadigh, Phys. Rev. Lett. **85**, 594 (2000).